Phosphodiesterase 4B in the cardiac L-type Ca^{2+} channel complex regulates Ca^{2+} current and protects against ventricular arrhythmias in mice

Jérôme Leroy,[1,2] Wito Richter,[3] Delphine Mika,[1,2] Liliana R.V. Castro,[1,2] Aniella Abi-Gerges,[1,2] Moses Xie,[3] Colleen Scheitrum,[3] Florence Lefebvre,[1,2] Julia Schittl,[1,2] Philippe Mateo,[1,2] Ruth Westenbroek,[4] William A. Catterall,[4] Flavien Charpentier,[5,6] Marco Conti,[3] Rodolphe Fischmeister,[1,2] and Grégoire Vandecasteele[1,2]

[1]INSERM UMR-S 769, Châtenay-Malabry, France. [2]University Paris-Sud, IFR141, Châtenay-Malabry, France. [3]Department of Obstetrics, Gynecology, and Reproductive Sciences, UCSF, San Francisco, California, USA. [4]Department of Pharmacology, University of Washington School of Medicine, Seattle, Washington, USA. [5]INSERM UMR-S915, CNRS ERL3147, l'institut du thorax, Nantes, France. [6]University of Nantes, Nantes, France.

β-Adrenergic receptors (β-ARs) enhance cardiac contractility by increasing cAMP levels and activating PKA. PKA increases Ca^{2+}-induced Ca^{2+} release via phosphorylation of L-type Ca^{2+} channels (LTCCs) and ryanodine receptor 2. Multiple cyclic nucleotide phosphodiesterases (PDEs) regulate local cAMP concentration in cardiomyocytes, with PDE4 being predominant for the control of β-AR–dependent cAMP signals. Three genes encoding PDE4 are expressed in mouse heart: *Pde4a*, *Pde4b*, and *Pde4d*. Here we show that both PDE4B and PDE4D are tethered to the LTCC in the mouse heart but that β-AR stimulation of the L-type Ca^{2+} current ($I_{Ca,L}$) is increased only in *Pde4b*$^{-/-}$ mice. A fraction of PDE4B colocalized with the LTCC along T-tubules in the mouse heart. Under β-AR stimulation, Ca^{2+} transients, cell contraction, and spontaneous Ca^{2+} release events were increased in *Pde4b*$^{-/-}$ and *Pde4d*$^{-/-}$ myocytes compared with those in WT myocytes. In vivo, after intraperitoneal injection of isoprenaline, catheter-mediated burst pacing triggered ventricular tachycardia in *Pde4b*$^{-/-}$ mice but not in WT mice. These results identify PDE4B in the $Ca_V1.2$ complex as a critical regulator of $I_{Ca,L}$ during β-AR stimulation and suggest that distinct PDE4 subtypes are important for normal regulation of Ca^{2+}-induced Ca^{2+} release in cardiomyocytes.

Introduction

During the cardiac action potential, Ca^{2+} influx through sarcolemmal L-type Ca^{2+} channels (LTCCs) triggers Ca^{2+} release from juxtaposed ryanodine receptor 2 (RyR2) located in the sarcoplasmic reticulum (SR). This allows a rapid and synchronous Ca^{2+} elevation throughout the cell, which activates contraction. During cardiac relaxation, Ca^{2+} is rapidly extruded by the Na^+/Ca^{2+} exchanger and re-sequestered into the SR by the Ca^{2+}-ATPase, SERCA2 (1). This process is highly regulated, in particular, by the sympathetic nervous system. β-Adrenergic receptors (β-ARs) exert strong inotropic and lusitropic effects by increasing intracellular cAMP levels and activating cAMP-dependent PKA. PKA then phosphorylates the key proteins of the excitation-contraction coupling (ECC) process, including LTCC and RyR2 but also phospholamban (PLB), which controls Ca^{2+} reuptake by SERCA2, as well as the myofilament proteins troponin I and myosin binding protein C (1).

The cardiac LTCC consists of the central pore-forming subunit α_{1C} ($Ca_V1.2$) and auxiliary β and α_2-δ subunits that modulate its function (2). Upon β-AR stimulation, phosphorylation of $Ca_V1.2$, the auxiliary β_2 subunit, or the closely associated protein AHNAK by PKA increases channel activity, thus enhancing the L-type Ca^{2+} current ($I_{Ca,L}$) (3–5). This regulation involves physical association of PKA with $Ca_V1.2$ via an A-kinase anchoring protein, AKAP15/18 (6, 7). Similarly, different AKAPs are responsible for the localization of PKA in the immediate vicinity of ECC proteins: the muscle-specific AKAP targets PKA to RyR2 (8, 9), and AKAP18δ localizes PKA to PLB (10).

PKA targeting by AKAPs would not be sufficient to explain hormonal specificity if cAMP could diffuse freely inside cells (11). In addition to discrete production sites, cAMP spreading is restricted by cyclic nucleotides phosphodiesterases (PDEs), the enzymes that degrade cAMP and cGMP into their inactive counterparts, 5′-AMP and 5′-GMP, respectively. Classically, 4 different PDE families (PDE1–PDE4) hydrolyze cAMP in heart: PDE1, which is activated by Ca^{2+}-calmodulin; PDE2, which is stimulated by cGMP; PDE3, which is inhibited by cGMP; and PDE4. PDE1 and PDE2 can hydrolyze both cAMP and cGMP, PDE3 preferentially hydrolyzes cAMP, and PDE4 is specific for cAMP (12). A fifth PDE, PDE8A, has been recently shown to modulate cAMP signaling in mouse cardiomyocytes (13). Association of individual PDE families to G_s-coupled receptors enables cardiac cells to generate heterogeneous cAMP signals in response to different hormones and specific control of $I_{Ca,L}$ (14).

PDE4 is one of the main PDEs expressed in heart. PDE4 becomes predominantly active upon β-AR stimulation and regulates global cAMP levels in cardiac cells (14–19). Particularly, PDE4 is the main PDE modulating $I_{Ca,L}$ in cardiomyocytes (18, 20). The PDE4 family is encoded by 4 genes (*PDE4A*–*PDE4D*), but only *PDE4A*, *PDE4B*,

Authorship note: Jérôme Leroy and Wito Richter contributed equally to this work.
Conflict of interest: The authors have declared that no conflict of interest exists.
Citation for this article: *J Clin Invest.* 2011;121(7):2651–2661. doi:10.1172/JCI44747.

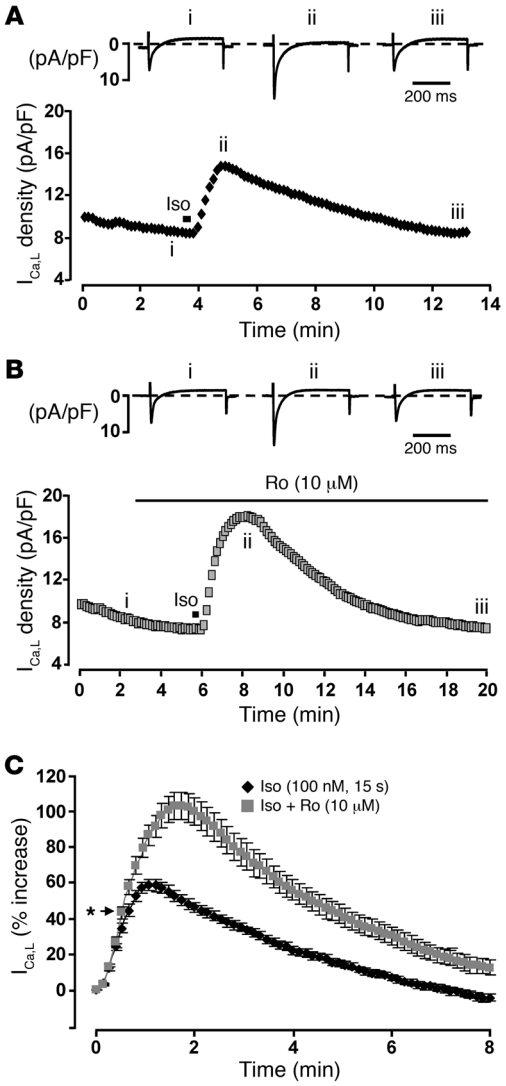

Figure 1
PDE4 modulates β-AR stimulation of $I_{Ca,L}$ in mouse ventricular myocytes. (**A**) Typical time course of $I_{Ca,L}$ amplitude in a cell stimulated by a 15-second pulse of Iso (100 nM). Each square represents the amplitude of $I_{Ca,L}$ recorded every 8 seconds during a depolarization from –50 to 0 mV. (**B**) $I_{Ca,L}$ was further increased when the cell was preincubated with the PDE4 inhibitor Ro 20-1724 (Ro; 10 μM) 2 minutes prior to the 15-second pulse of Iso (100 nM) and maintained throughout the experiment. The individual current traces shown on top of **A** and **B** were recorded at the times indicated by the corresponding roman numerals in the graphs below. (**C**) Mean variation of $I_{Ca,L}$ after Iso (100 nM, 15 seconds) application alone (black diamonds; $n = 62$ myocytes) or when PDE4 was inhibited by Ro 20-1724 (gray squares; $n = 37$ myocytes). All curves represent the mean ± SEM. *$P < 0.05$ indicates the first of the statistically significant points on the graph. All points that occur after this time point are significant.

and *PDE4D* are expressed in cardiac tissue (21). These 3 genes give rise to multiple isoforms generated through alternative splicing and by the use of different promoters (22). So far, of these genes, most of our knowledge in the heart concerns the *PDE4D* gene. Long variants of this gene expressed in the heart include the isoforms PDE4D3, PDE4D5, PDE4D8, and PDE4D9 (23, 24). PDE4D5, PDE4D8, and PDE4D9 were shown to differentially interact with β_1-AR and β_2-AR subtypes in neonatal cardiomyocytes, either directly or by binding to β-arrestin (25–27). The PDE4D3 isoform was found in macromolecular signaling complexes, regulating 2 major players of ECC: KCNQ1/KCNE1 potassium channels (28) and RyR2 (29). In *Pde4d*$^{-/-}$ mice, RyR2 is hyperphosphorylated by PKA, leading to abnormal Ca^{2+} release, increased sensitivity to exercise-induced arrhythmias, and development of a late-onset dilated cardiomyopathy (29). In addition, a long PDE4D variant was recently found to associate with SERCA2 in the heart (30).

We believe that until now, the molecular identity of the PDE4 regulating the LTCC was unknown. Because of the prominent role of PDE4D variants in the β-AR cascade, we anticipated that a PDE4D variant might also regulate the LTCC activity. Our initial goal here was to test this hypothesis. We indeed found that PDE4D is part of a $Ca_V1.2$ signaling complex, but, to our surprise, inactivation of the *Pde4d* gene had no consequence on basal or β-AR stimulated $I_{Ca,L}$, although Ca^{2+} transients and contraction were enhanced. We therefore explored the role of the 2 other cardiac PDE4 isoforms, PDE4A and PDE4B, and found that PDE4B, but not PDE4A, was also associated with the LTCC. In *Pde4b*$^{-/-}$ mice, but not in *Pde4a*$^{-/-}$ mice, the β-AR response of $I_{Ca,L}$ was increased, together with an increase in cell contraction and Ca^{2+} transients. In vivo, upon β-AR stimulation, catheter-mediated burst pacing triggered ventricular tachycardia (VT) in *Pde4b*$^{-/-}$ mice but not in WT mice. We conclude that not only PDE4D, but also PDE4B, plays a key role during β-AR stimulation of cardiac function. PDE4B, by limiting the amount of Ca^{2+} that enters the cell via the LTCCs, prevents Ca^{2+} overload and arrhythmias.

Results

β-AR stimulation of $I_{Ca,L}$ and effect of PDE4 inhibition in adult mouse ventricular myocytes. We previously showed that the β-AR stimulation of $I_{Ca,L}$ is under the control of PDE4 in adult rat ventricular myocytes (18). To determine whether the same was true in mice, $I_{Ca,L}$ was recorded in adult mouse ventricular myocytes (AMVMs) using the whole-cell patch-clamp technique, and the response of this current to a short application of the nonselective β-AR agonist isoprenaline (Iso) was studied. As shown in Figure 1A, a 15-second stimulation with 100 nM Iso elicited a rapid and transient increase of $I_{Ca,L}$ amplitude that returned to baseline in less than 10 minutes. Selective PDE4 inhibition with Ro 20-1724 (10 μM) had no effect on basal $I_{Ca,L}$ but strongly potentiated the stimulation of the current by Iso (Figure 1B). On average, Iso alone increased $I_{Ca,L}$ maximally by 58.8% ± 3.3% ($n = 62$; Figure 1C). When PDE4 was inhibited, the stimulatory effect of Iso was prolonged, and the maximal stimulation of $I_{Ca,L}$ reached 103.3% ± 7.7% ($n = 37$; Figure 1C; $P < 0.001$ vs. Iso alone). These results identify PDE4 as an important negative-feedback mechanism of the β-AR regulation of $I_{Ca,L}$ in AMVMs.

Characterization of PDE4 subtypes in mouse heart. To evaluate the contribution of PDE4 to cAMP hydrolysis in the mouse heart, total cAMP hydrolytic activity was measured in ventricle homogenates, and the fraction corresponding to PDE4 was assessed with the specific inhibitor rolipram. As shown in Figure 2A, PDE4 represented about 33% of the total activity. To further dissect the contributions of single PDE4 subtypes to the total PDE4 activity, heart extracts were immunoprecipitated using subtype-specific antibodies

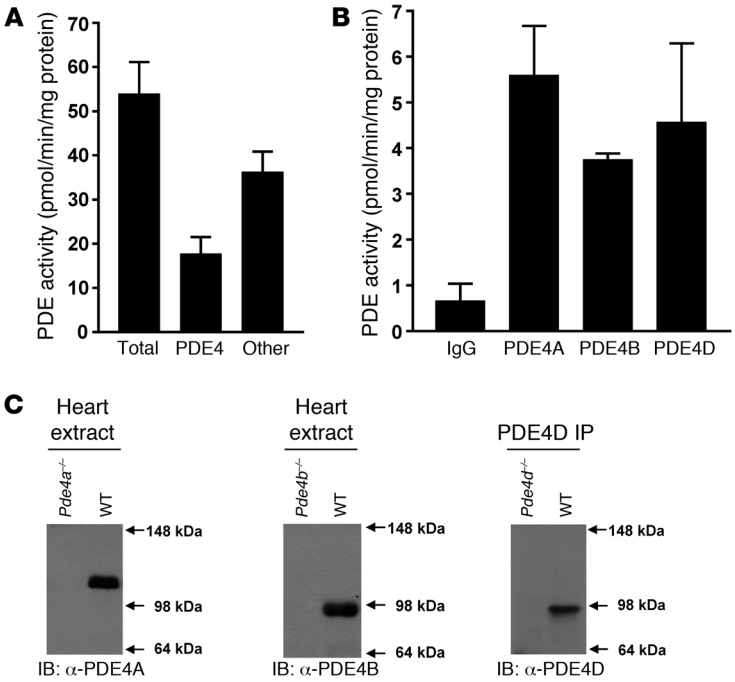

Figure 2
Characterization of PDE4 activity and subtypes in the adult mouse heart. (**A**) Heart protein extracts were assayed using 1 μM cAMP as substrate. PDE4 activity is defined as the fraction of total PDE activity inhibited by the specific PDE4 inhibitor rolipram (10 μM). (**B**) Cardiac extracts were immunoprecipitated with control IgG or using antibodies specific for PDE4A, PDE4B, or PDE4D. The graph shows the PDE activity in the IP pellet using 1 μM cAMP as substrate. Data represent the mean ± SEM of experiments performed at least 3 times. (**C**) Heart protein extracts from WT mice, *Pde4a*$^{-/-}$ mice, and *Pde4b*$^{-/-}$ mice were separated on SDS/PAGE and revealed with the corresponding PDE4 subtype-specific antibodies. In the case of PDE4D, cardiac extracts from WT and *Pde4d*$^{-/-}$ were first immunoprecipitated with the specific PDE4D antibody and then revealed by Western blot.

against PDE4A, PDE4B, and PDE4D (23), and the PDE activity recovered in the IP pellets was assayed. As shown in Figure 2B, the activities of PDE4A, PDE4B, and PDE4D were comparable in the mouse heart. Western blot experiments indicated that each of these activities results from the expression of long PDE4 variants detected as one major immunoreactive band. The absence of signal in mice deficient for the corresponding gene demonstrates that the antibodies used are specific (Figure 2C).

PDE4B and PDE4D are part of the L-type calcium channel complex. To determine whether any of these PDE4 associate with the LTCC, we performed IP experiments using mouse heart extracts. The pore-forming subunits of the channel, $Ca_V1.2$, were immunoprecipitated with an anti-$Ca_V1.2$ antibody (31). A cAMP-hydrolyzing PDE4 activity was associated with the IP Ca^{2+} channel subunit from WT cardiac tissue and was unaffected in heart extracts from *Pde4a*$^{-/-}$ mice. In contrast, this PDE4 activity was significantly decreased in ventricular tissues from *Pde4b*$^{-/-}$ and *Pde4d*$^{-/-}$ mice (Figure 3A). This suggests that PDE4B and PDE4D are part of a macromolecular complex that includes the LTCC, a finding confirmed by Western blot analysis of $Ca_V1.2$ IP pellets. Using specific isoform antibodies, both PDE4B (Figure 3B) and PDE4D (Figure 3C) were detected in the cardiac LTCC complex. These interactions were specific, because both enzymes were excluded from IPs using control IgGs (Figure 3, B and C). Furthermore, PDE4B could not be detected in the $Ca_V1.2$ complex in hearts from *Pde4b*$^{-/-}$ mice, and the same was true for PDE4D when the coimmunoprecipitation experiment was performed in hearts from *Pde4d*$^{-/-}$ mice. This demonstrates that both PDE4B and PDE4D isoforms associate with $Ca_V1.2$ in the heart and are part of a macromolecular signaling complex, including the cardiac LTCC.

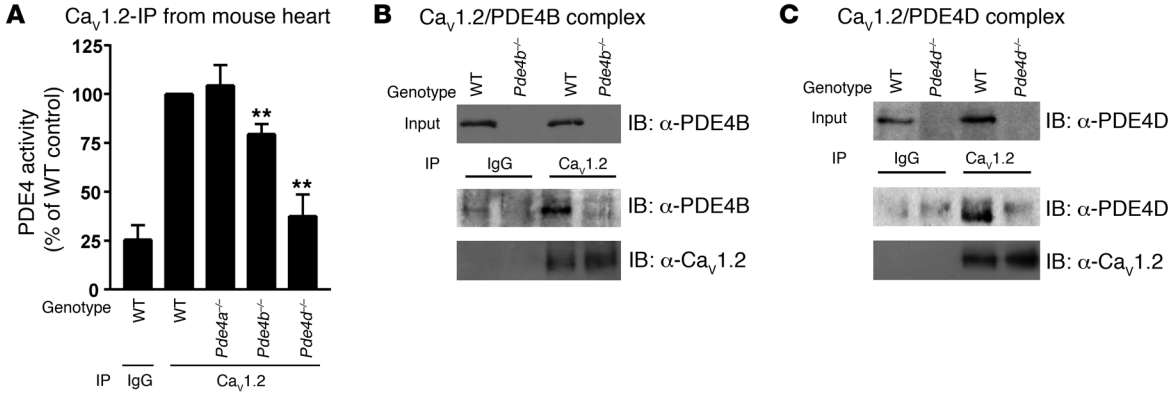

Figure 3
PDE4B and PDE4D are part of the LTCC complex. (**A**) $Ca_V1.2$ was immunoprecipitated from cardiac homogenates of WT mice, *Pde4a*$^{-/-}$, *Pde4b*$^{-/-}$, and *Pde4d*$^{-/-}$ mice. The associated PDE4 activity was assessed using rolipram. $^{**}P < 0.01$. (**B**) PDE4B was detected in cardiac lysates from WT animals and coimmunoprecipitated with $Ca_V1.2$. (**C**) PDE4D was also detected in cardiac lysates from WT animals and was associated with $Ca_V1.2$. IP IgG, negative control. Data are representative of at least 3 independent experiments.

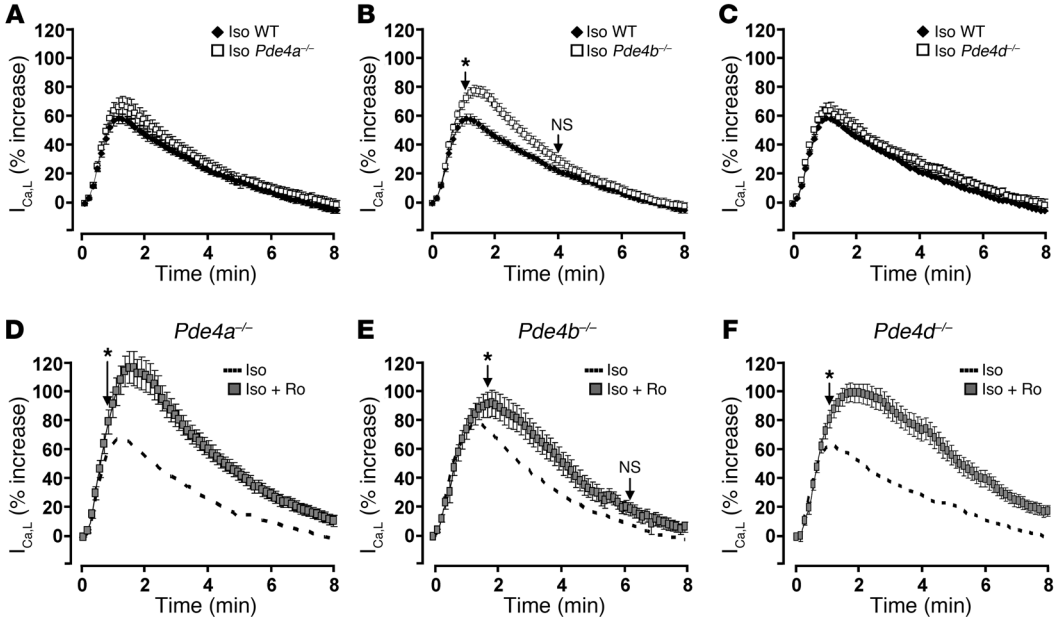

Figure 4

Pde4b inactivation potentiates the β-AR stimulation of the $I_{Ca,L}$ in AMVMs. (**A**–**C**) Average time course of $I_{Ca,L}$ amplitude after a brief β-AR stimulation induced by Iso (100 nM, 15 seconds) in WT AMVMs (black squares; $n = 62$ cells) and PDE4-deficient AMVMs (white squares) (*Pde4a*$^{-/-}$, $n = 29$ cells; *Pde4b*$^{-/-}$, $n = 46$ cells; *Pde4d*$^{-/-}$, $n = 31$ cells). (**D**–**F**) Effect of global PDE4 inhibition with 10 μM Ro 20-1724 on $I_{Ca,L}$ stimulation induced by Iso (100 nM, 15 seconds) in PDE4-deficient AMVMs (*Pde4a*$^{-/-}$, $n = 24$ cells; *Pde4b*$^{-/-}$, $n = 22$ cells; *Pde4d*$^{-/-}$, $n = 28$ cells). Ro 20-1724 was applied 2 minutes prior to the β-AR stimulation and maintained throughout the experiment (gray squares). For comparison, dashed lines indicate the effect of Iso alone on $I_{Ca,L}$ in the corresponding genotypes. All graphs are average ± SEM. *$P < 0.05$ indicates the first of the statistically significant points on each graph. All points that occur after those time points are significant.

β-*AR stimulation of* $I_{Ca,L}$ *and effect of PDE4 inhibition in PDE4-deficient mice.* To assess the respective contribution of PDE4A, PDE4B, and PDE4D in the β-AR regulation of $I_{Ca,L}$, patch-clamp experiments were performed in AMVMs isolated from mice deficient in the corresponding genes (*Pde4a*$^{-/-}$, *Pde4b*$^{-/-}$, and *Pde4d*$^{-/-}$ mice). Cell capacitance and $I_{Ca,L}$ amplitude at baseline were similar in ventricular myocytes from each genotype. As shown in Figure 4A, $I_{Ca,L}$ potentiation by Iso (100 nM, 15 seconds) was unchanged in *Pde4a*$^{-/-}$ compared to that in WT AMVMs. Unexpectedly, the same was true for myocytes isolated from *Pde4d*$^{-/-}$ mice (Figure 4C). In line with these results, the PDE4 inhibitor Ro 20-1724 (10 μM) strongly enhanced the effect of Iso on $I_{Ca,L}$ in *Pde4a*$^{-/-}$ and *Pde4d*$^{-/-}$ mice (Figure 4, D and F), and this effect was not different from that obtained in WT mice (compare Figure 4, D and F, with Figure 1C), suggesting that these isoforms do not modulate the β-AR stimulation of $I_{Ca,L}$. In contrast, the response of $I_{Ca,L}$ to a transient β-AR stimulation was significantly enhanced in ventricular myocytes isolated from *Pde4b*$^{-/-}$ mice compared with that from WT mice (Figure 4B, maximal $I_{Ca,L}$ potentiation by Iso was 78.3% ± 3.6% in *Pde4b*$^{-/-}$ mice, $n = 46$; $P < 0.001$ vs. WT). Moreover, the effect of Ro 20-1724 was severely blunted in *Pde4b*$^{-/-}$ myocytes (Figure 4E). These findings indicate that PDE4B is the predominant PDE4 isoform involved in $I_{Ca,L}$ regulation by short β-AR stimulation in mice. However, since the effect of Ro 20-1724 was not completely abolished in *Pde4b*$^{-/-}$ mice, another PDE4 isoform must be involved in the β-AR regulation of $I_{Ca,L}$, at least when PDE4B is absent. This is most likely PDE4D, since this isoform was also found to coimmunoprecipitate with the pore-forming subunit of $Ca_V1.2$ (Figure 3, A and C). The biophysical properties of $I_{Ca,L}$ were compared in WT and *Pde4b*$^{-/-}$ myocytes. As shown in Figure 5A, the current-voltage relationship revealed a similar $I_{Ca,L}$ density measured in WT and *Pde4b*$^{-/-}$ myocytes under basal conditions. $I_{Ca,L}$ exhibited similar voltage dependence in both genotypes: the half-time for activation and inactivation remained unchanged (Figure 5B). When measured at 0 mV, $I_{Ca,L}$ amplitude, upon continuous application of Iso at a submaximal concentration (3 nM), was significantly increased in WT AMVMs, from 5.9 ± 0.4 pA/pF to 7.3 ± 0.6 pA/pF ($P < 0.05$), but the β-AR stimulation induced a greater increase of $I_{Ca,L}$ amplitude in *Pde4b*$^{-/-}$ myocytes than in WT myocytes (Figure 5C). This increase was accompanied by a pronounced leftward shift of the activation curve of $I_{Ca,L}$ in *Pde4b*$^{-/-}$ myocytes, whereas steady-state inactivation was not modified (Figure 5D). As a consequence, under β-AR stimulation, the "window" current between –30 mV and 0 mV was enhanced in myocytes lacking PDE4B.

Colocalization of PDE4B and $Ca_V1.2$ *channels at the Z-line in AMVMs.* We next determined the subcellular localization of PDE4B in AMVMs and examined whether PDE4B and $Ca_V1.2$ colocalize in vivo by using the double-labeling immunofluorescence technique. In agreement with previous studies (7, 32), the staining for $Ca_V1.2$ obtained with the anti-$Ca_V1.2$ antibody was observed as a regularly spaced, punctuated pattern, which overlapped with the Z-line marker α-actinin (Figure 6A). Immunolabeling of PDE4B with an antibody that specifically recognizes this isoform (Figure 2C) revealed a strong fluorescent signal throughout the cell and a tight, striated pattern, with the main intensity stripe overlapping with α-actinin (Figure 6B). In AMVMs isolated from *Pde4b*$^{-/-}$ hearts, the overall staining intensity for PDE4B was reduced, and, notably, the striation that had overlapped with α-actinin in WT

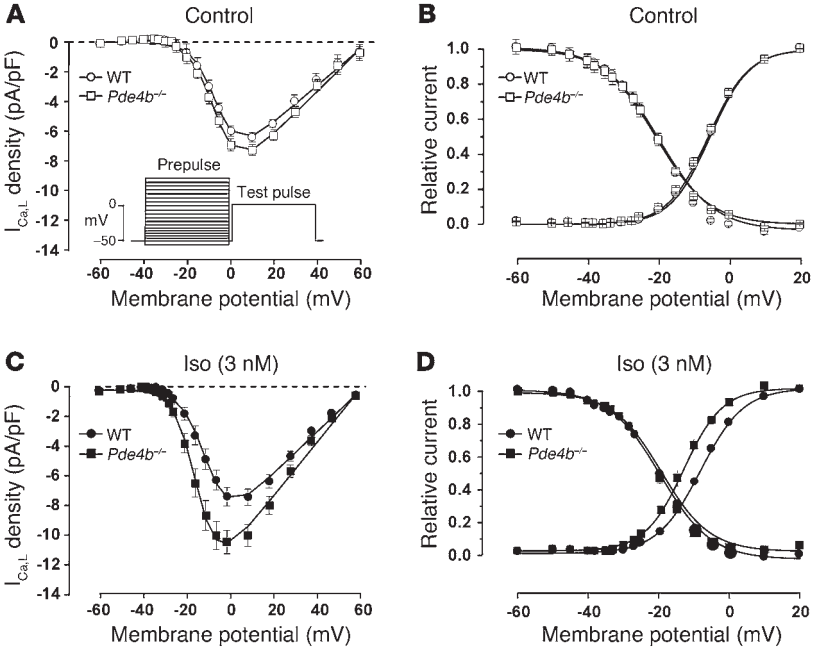

Figure 5

Pde4b ablation increases LTCC window current upon β-AR stimulation. (**A**) Mean $I_{Ca,L}$ density elicited by depolarizing steps from a holding potential of –50 mV, using a double-pulse protocol (inset), was similar in WT (n = 15 cells) and *Pde4b*$^{-/-}$ (n = 16 cells) AMVMs under control conditions. (**B**) Combined activation and steady-state inactivation curves under control conditions illustrate window current of $I_{Ca,L}$ (half-time for activation [$V_{1/2,\,act}$] = –6.1 ± 0.9 mV, k = 5.4 ± 0.1 mV in *Pde4b*$^{-/-}$ AMVMs and $V_{½,\,act}$ = –5.6 ± 0.7 mV, k = 5.4 ± 0.2 mV in WT [NS]; half-time for inactivation [$V_{1/2,\,inact}$] = –21.7 ± 0.8 mV, k = 7.1 ± 0.3 mV in *Pde4b*$^{-/-}$ AMVMs and –21.9 ± 0.9 mV, k = 6.4 ± 0.3 mV in WT [NS]. (**C**) $I_{Ca,L}$ density recorded during depolarizing pulses from –50 mV was further potentiated in *Pde4b*$^{-/-}$ (n = 14) versus WT (n = 16) AMVMs upon sustained β-AR stimulation (3 nM Iso). (**D**) Increased $I_{Ca,L}$ window current upon β-AR stimulation in *Pde4b*$^{-/-}$ AMVMs. Activation curve of $I_{Ca,L}$ was more hyperpolarized upon Iso (3 nM) application in *Pde4b*$^{-/-}$ AMVMs ($V_{1/2,\,act}$ = –12.2 ± 1.2 mV, k = 5.3 ± 0.2 mV) than in WT AMVMs ($V_{1/2,\,act}$ = –7.5 ± 1.3 mV, k = 5.4 ± 0.2 mV, P < 0.05); inactivation was not affected by β-AR stimulation in either genotype ($V_{1/2,\,inact}$ = –21.7 ± 0.4 mV, k = 6.2 ± 0.4 mV in *Pde4b*$^{-/-}$ and $V_{1/2,\,inact}$ = –21.3 ± 0.7 mV, k = 6.3 ± 0.2 mV in WT).

myocytes was absent (Figure 6C). Our interpretation of these results is that $Ca_V1.2$ and a fraction of PDE4B are colocalized along T-tubule membranes in AMVMs.

β-AR regulation of ECC in AMVMs from Pde4b$^{-/-}$ *and Pde4d*$^{-/-}$ *mice.* The fact that PDE4B modulates the β-AR stimulation of $I_{Ca,L}$ and PDE4D regulates RyR2 (29) prompted us to compare the ECC process in WT, *Pde4b*$^{-/-}$, and *Pde4d*$^{-/-}$ mice. For this, sarcomere length (SL) and intracellular Ca^{2+} were recorded simultaneously in Fura-2–loaded ventricular myocytes paced at 0.5 Hz. As shown in Figure 7, A and B, under nonstimulated basal conditions, SL shortening and Ca^{2+} transient amplitude were similar in the 3 genetic backgrounds. In WT, *Pde4b*$^{-/-}$, and *Pde4d*$^{-/-}$ cells, pulse stimulation with Iso (100 nM, 15 seconds) strongly increased SL shortening and Ca^{2+} transient amplitude. However, these effects were more pronounced in PDE4-deficient myocytes: maximal shortening measured at the peak of Iso stimulation was increased by about 50% in *Pde4b*$^{-/-}$ (n = 47) and *Pde4d*$^{-/-}$ (n = 47) myocytes compared with that in WT myocytes (n = 51, P < 0.001), whereas Ca^{2+} transient amplitude was increased by about 25% and 28% more in *Pde4b*$^{-/-}$ (n = 47) and *Pde4d*$^{-/-}$ myocytes (n = 47), respectively, than in WT myocytes (n = 51; P < 0.01). Figure 7C shows the corresponding kinetics of relaxation and decay of the Ca^{2+} transients. In basal conditions, there was no difference in time to half maximal decay ($t_{1/2off}$) values of relaxation and Ca^{2+} transient decay among the different genotypes. Iso strongly accelerated relaxation ($t_{1/2off}$ values were decreased by about 65%) and Ca^{2+} transient decay ($t_{1/2off}$ values were decreased by about 57%) in WT myocytes (n = 51). In *Pde4b*$^{-/-}$ and *Pde4d*$^{-/-}$ myocytes (n = 47 each) relaxation was further accelerated ($t_{1/2off}$ values were decreased by about 81% and 78% of basal value, respectively; P < 0.001 vs. WT), whereas decay kinetics of the Ca^{2+} transients in the presence of Iso were not significantly different from those of WT myocytes (Figure 7C). However, the decay phase of Ca^{2+} transients tended to be accelerated in *Pde4b*$^{-/-}$ myocytes compared with WT myocytes (P = 0.059), and the difference was significant compared with *Pde4d*$^{-/-}$ myocytes (P < 0.05). As shown in Figure 7, D and E, *Pde4b*$^{-/-}$ and *Pde4d*$^{-/-}$ myocytes also displayed increased spontaneous Ca^{2+} release (SCR) events upon Iso stimulation. On average, during a 20-second period after the maximal effect of Iso stimulation, 4.5 ± 1.1 SCR events occurred in *Pde4b*$^{-/-}$ myocytes (n = 47), and 4.5 ± 0.9 SCR events occurred in *Pde4d*$^{-/-}$ myocytes (n = 47), whereas in WT cells, only 1.4 ± 0.5 SCR events were observed (n = 51; P < 0.01). These results show that both PDE4B and PDE4D are required for normal regulation of ECC during β-AR stimulation. To further examine the consequences of PDE4B and PDE4D ablation on SR function, we measured SR Ca^{2+} load by fast application of 10 mM caffeine in basal conditions and at the peak of Iso (100 nM, 15 seconds) stimulation. As shown in the Supplemental Figure 1, A and B (supplemental material available online with this article; doi:10.1172/JCI44747DS1), SR Ca^{2+} load was not significantly different in the 3 genotypes. However, there was a tendency for a decreased SR Ca^{2+} load in *Pde4d*$^{-/-}$ myocytes in basal conditions (–20%). As a consequence, the percentage increase in SR Ca^{2+} load induced by Iso was significantly higher in *Pde4d*$^{-/-}$ myocytes versus WT myocytes (P < 0.05, n = 18 each; Supplemental Figure 1C). We thus examined PLB phosphorylation at Ser-16 (PKA site) in isolated myocytes from the 3 genotypes. PLB phosphorylation was not different in the 2 groups under basal conditions. After Iso challenge (100 nM, 15 seconds), PLB phosphorylation was significantly increased in *Pde4d*$^{-/-}$ myocytes compared with that in WT myocytes, and a nonsignificant increase was observed in *Pde4b*$^{-/-}$ myocytes (Supplemental Figure 1D).

ECG, intracardiac recording, and pacing. The arrhythmic behavior of *Pde4b*$^{-/-}$ myocytes and the increased susceptibility of *Pde4d*$^{-/-}$ mice to exercise-induced cardiac arrhythmias (29) prompted us to evaluate the propensity to ventricular arrhythmias in *Pde4b*$^{-/-}$ mice. Six-lead ECGs were recorded in 10 WT and 11 *Pde4b*$^{-/-}$ mice (mean age of 17 ± 1 weeks in both groups) in baseline conditions. No significant differences were observed in RR interval (WT, 128 ± 7 ms; *Pde4b*$^{-/-}$, 114 ± 7 ms), P wave (WT, 14 ± 1 ms; *Pde4b*$^{-/-}$, 11 ± 1

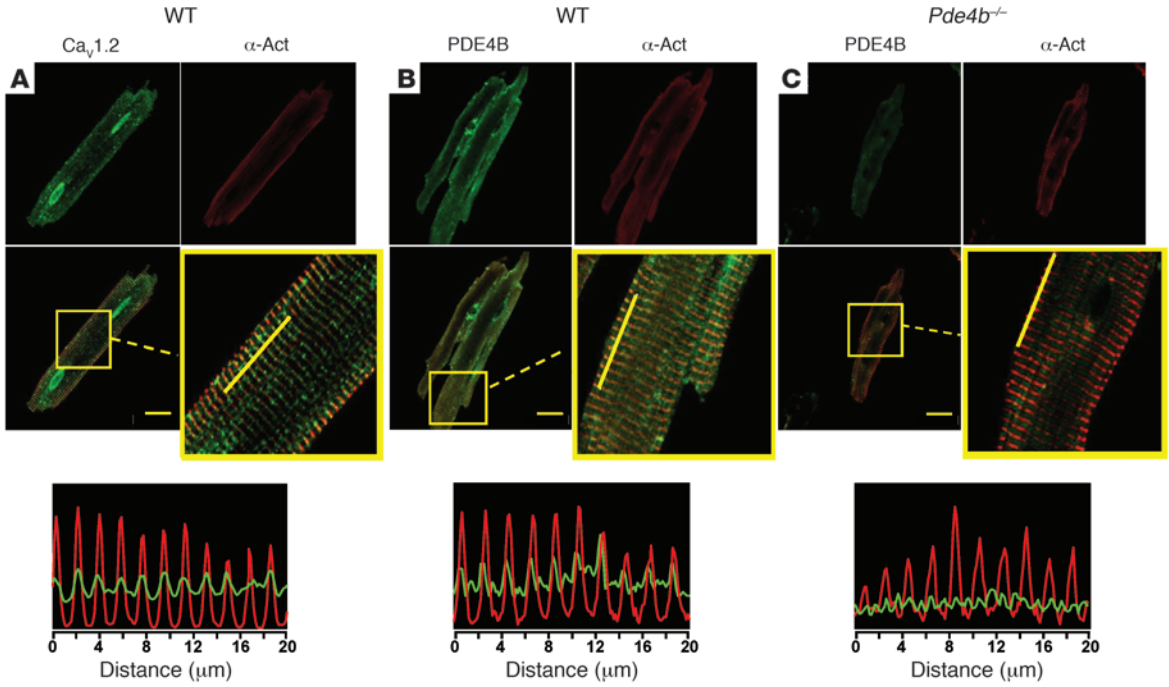

Figure 6
Localization of PDE4B and LTCC at the transverse tubules in AMVMs. (**A**) Confocal images of a WT AMVM double labeled with anti-$Ca_V1.2$ antibody (CNC1, green) and anti–α-actinin antibody (α-Act, red). (**B**) Confocal images of a WT AMVM double labeled with anti-PDE4B antibody (green) and anti–α-actinin antibody (red). (**C**) Confocal images of a *Pde4b*$^{-/-}$ AMVM double labeled with anti-PDE4B antibody (green) and anti–α-actinin antibody (red). Scale bar: 20 μm. The graph below each panel indicates the relative fluorescence intensities in the green and red channels measured along a 20-μm distance, as indicated by the yellow line on the enlarged boxed area from the merged images.

ms), PQ interval (WT, 39 ± 1 ms; *Pde4b*$^{-/-}$, 37 ± 1 ms), QRS complex (WT, 12 ± 1 ms; *Pde4b*$^{-/-}$, 11 ± 1 ms), and QTc interval (WT, 47 ± 2 ms; *Pde4b*$^{-/-}$, 50 ± 3 ms) durations. These mice were then used for catheter-mediated ventricular pacing in baseline conditions and after intraperitoneal injections of Iso (0.02 mg/kg and 0.2 mg/kg). Two mice (1 per group) died during the experimental procedure and were excluded from the statistical analysis. In baseline conditions, intracardiac ECG recordings in WT and *Pde4b*$^{-/-}$ mice were similar. *Pde4b* inactivation had no significant effect on the ventricular effective refractory period (VERP) measured at a basic cycle length of 75 ms (WT, 44 ± 2 ms; *Pde4b*$^{-/-}$, 40 ± 2 ms; NS). Iso decreased spontaneous RR interval from 118 ± 5 ms in baseline to 93 ± 4 ms and 90 ± 1 ms at 0.02 mg/kg Iso and 0.2 mg/kg Iso, respectively, in WT mice ($P < 0.001$ vs. baseline for both doses) and from 109 ± 5 ms to 88 ± 2 ms and 87 ± 1 ms, respectively, in *Pde4b*$^{-/-}$ mice ($P < 0.001$ vs. baseline for both doses; P = NS vs. WT). VERP was reduced to 38 ± 3 ms and 34 ± 3 ms after injection of Iso at, respectively, 0.02 mg/kg and 0.2 mg/kg ($P < 0.001$ and $P < 0.05$ vs. baseline) in WT mice and to 34 ± 2 ms and 32 ± 3 ms, respectively, in *Pde4b*$^{-/-}$ mice ($P < 0.01$ and $P < 0.05$ vs. baseline; P = NS vs. WT). Other ECG parameters were similar in the 2 groups (data not shown). In baseline conditions, burst pacing did not induce arrhythmias either in WT or in *Pde4b*$^{-/-}$ mice. However, after pretreatment with Iso, *Pde4b*$^{-/-}$ mice responded differently from WT mice. Indeed, burst pacing induced arrhythmias in *Pde4b*$^{-/-}$ mice in 1 out of 10 mice at 0.02 mg/kg Iso (P = NS vs. WT) and 4 out of 10 mice at 0.2 mg/kg Iso ($P < 0.05$ vs. WT; Figure 8, A and B) but not in WT mice. VT was induced in the 4 responding *Pde4b*$^{-/-}$ mice. Two of them had sustained VT. Thus, after treatment with Iso, *Pde4b* gene inactivation favored the occurrence of arrhythmias induced by burst pacing. In contrast, paced extrasystoles induced arrhythmias in both WT and *Pde4b*$^{-/-}$ mice (Figure 8C), with a moderately, though not significantly, higher incidence in *Pde4b*$^{-/-}$ mice.

Discussion

PDE4 is the predominant PDE family that controls cAMP and LTCC in rodent cardiomyocytes. In the present study, we show that *Pde4a*, *Pde4b*, and *Pde4d* are expressed in mouse heart, but only PDE4B and PDE4D are associated with $Ca_V1.2$ channels. Whereas β-AR stimulation of $I_{Ca,L}$ is normal in *Pde4a*$^{-/-}$ and *Pde4d*$^{-/-}$ myocytes, the β-AR responses of $I_{Ca,L}$, Ca^{2+} transients, and contraction are enhanced in myocytes from *Pde4b*$^{-/-}$ mice, and this is accompanied by an increased propensity for arrhythmia. β-AR stimulation of Ca^{2+} transients and contraction are also enhanced in myocytes from *Pde4d*$^{-/-}$ mice independently of $I_{Ca,L}$. For the first time to our knowledge, our results identify PDE4B as a major regulator of $I_{Ca,L}$ and cardiac function and suggest that PDE4B and PDE4D regulate ECC by different mechanisms.

In mouse ventricular myocytes, pharmacological inhibition of PDE4 does not affect basal $I_{Ca,L}$ but strongly enhances the effect of β-AR stimulation (Figure 1). A similar regulation of $I_{Ca,L}$ by PDE4 was found previously in human atrial and rat ventricular myocytes, thus clearly indicating that PDE4 is a major negative regulator of $I_{Ca,L}$ in the heart (14, 20, 33). Similar to what was reported earlier in the rat (34), PDE4 activity in the mouse ventricle was due to the expression of PDE4A, PDE4B, and PDE4D variants. The migra-

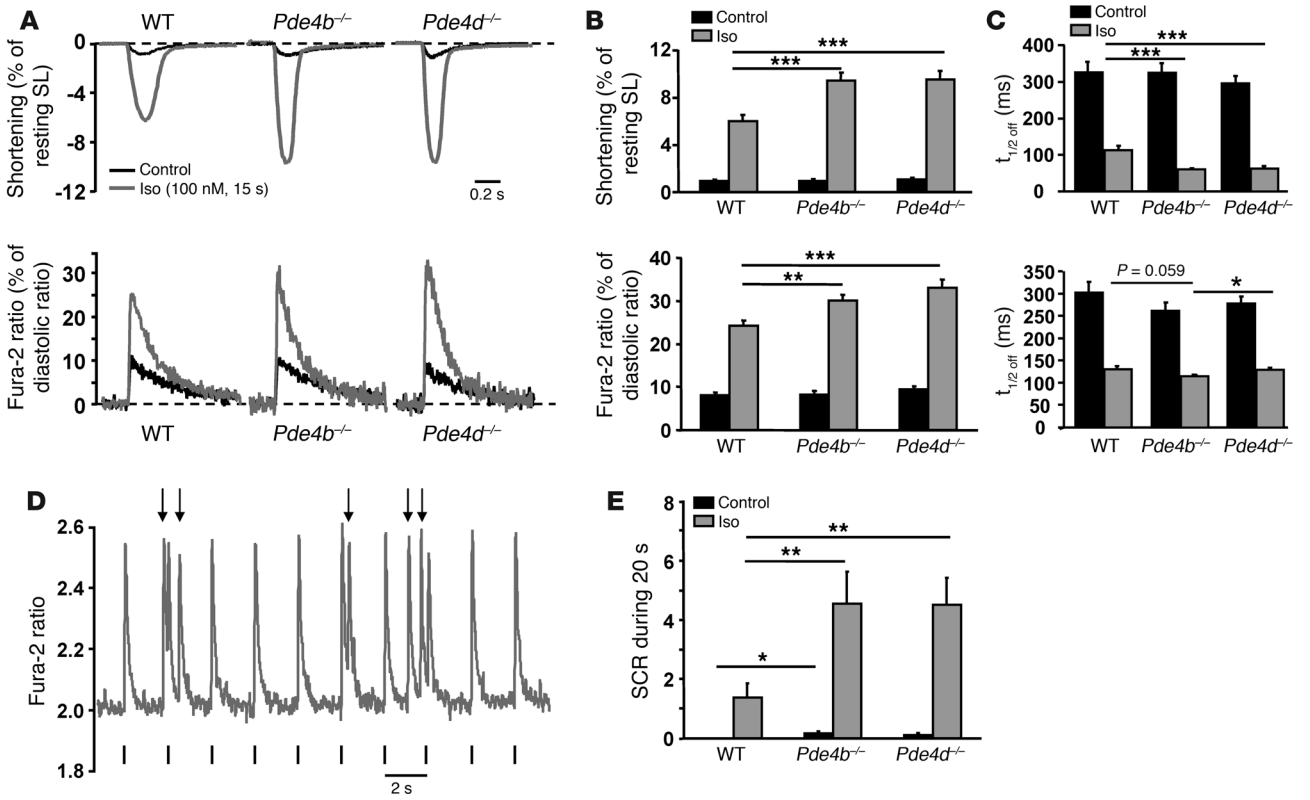

Figure 7

Enhanced ECC and increased arrhythmias upon transient β-AR stimulation in *Pde4b*$^{-/-}$ and *Pde4d*$^{-/-}$ mice. (**A**) Representative traces of sarcomere shortening (top) and Ca^{2+} transients (bottom) recorded in electrically paced (0.5 Hz) AMVMs from WT, *Pde4b*$^{-/-}$, and *Pde4d*$^{-/-}$ mice. The black traces correspond to control conditions, and the gray traces correspond to the maximal effect produced by a 15-second pulse of Iso (100 nM). (**B**) Mean data for sarcomere shortening (expressed as the percentage of resting length) and Fura-2 ratio (expressed as the percentage of diastolic ratio) variation measured in control conditions (black) and at the maximum of Iso stimulation (gray) measured in AMVMs from WT ($n = 51$), *Pde4b*$^{-/-}$ ($n = 47$), and *Pde4d*$^{-/-}$ ($n = 47$) mice. (**C**) Average $t_{1/2off}$ values for relaxation (top graph) and Ca^{2+} transient decay (bottom graph) in control conditions (black) and after Iso stimulation (gray) measured in AMVMs from WT ($n = 51$), *Pde4b*$^{-/-}$ ($n = 47$), and *Pde4d*$^{-/-}$ ($n = 47$) mice. (**D**) A representative trace of SCR events (arrows) induced by Iso in a *Pde4b*$^{-/-}$ AMVM paced at 0.5 Hz. (**E**) Bar graph representing the average number of SCR events during a 20-second period preceding the application of Iso (black) and an equally long period after the peak of the Iso effect (gray) in WT ($n = 51$), *Pde4b*$^{-/-}$ ($n = 47$), and *Pde4d*$^{-/-}$ ($n = 47$) AMVMs. Bar graphs represent the mean ± SEM. *$P < 0.05$; **$P < 0.01$; ***$P < 0.001$.

tion on SDS/PAGE of these variants corresponds to long forms, and although only one immunoreactive band was detected in each case, this band may correspond to the comigration of several long forms, as demonstrated earlier for PDE4D (23, 24, 29).

Specific variants of PDE4D have been shown to be associated with cardiac ion channels. Indeed, PDE4D3 was found to be coupled to RyR2 (29) and to be included in a macromolecular complex together with the KCNQ1 subunit of a potassium channel regulated by cAMP (28). Here, we found that PDE4D is also associated with the $Ca_V1.2$ subunit of the LTCC but, surprisingly, does not seem to regulate the channel activity, at least under normal conditions, because inactivation of the *Pde4d* gene modified neither $I_{Ca,L}$ nor its β-AR regulation. Since PDE4B was also found in the complex that includes the $Ca_V1.2$ subunit, and β-AR stimulation of $I_{Ca,L}$ is upregulated in *Pde4b*$^{-/-}$ mice, it is possible that PDE4B is more tightly coupled with the LTCC, hence controlling its phosphorylation, while PDE4D is more remote. This hypothesis is supported by the observation that the PDE4 inhibitor Ro 20-1724 had a small but significant effect on the β-AR response of $I_{Ca,L}$ in *Pde4b*$^{-/-}$ mice (Figure 4E), as if the effect of PDE4D were unmasked in the absence of PDE4B. PDE4D isoforms have been shown previously to interact with β-ARs (25–27). Since β-ARs are part of a signalosome, including the LTCCs (35), it is conceivable that the 2 PDE4 isoforms that immunoprecipitated with $Ca_V1.2$ are in fact located at different ends of the signalosome, with PDE4D associated with the β-AR and PDE4B associated with the LTCC. Alternatively, PDE4D and PDE4B may control different pools of $Ca_V1.2$ (36), the latter being responsible for Iso-dependent $I_{Ca,L}$ regulation.

Since LTCCs are predominantly expressed in the T-tubules (7, 32), PDE4B should be located in the same compartment. Consistent with this idea, immunocytochemical experiments with a specific PDE4B antibody revealed a strong staining at the Z-line in WT myocytes but not in *Pde4b*$^{-/-}$ myocytes (Figure 6). This indicates that PDE4B is enriched in the T-tubules, at variance with that found in neonatal rat cardiomyocytes (16). This discrepancy could be due to either interspecies differences or to the higher level of differentiation of adult cardiomyocytes.

$I_{Ca,L}$ constitutes the trigger for Ca^{2+}-induced Ca^{2+} release and cardiac contraction, and its size dictates the amplitude of Ca^{2+} transients and contraction (37, 38). Accordingly, Ca^{2+} transients

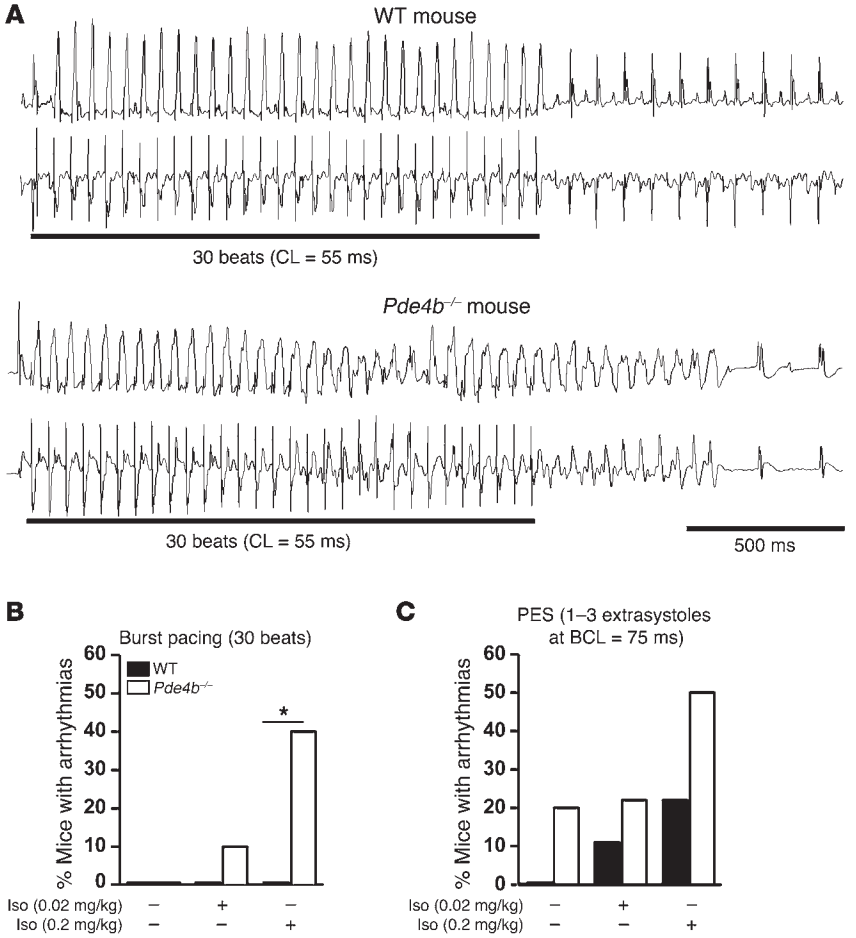

Figure 8
Increased susceptibility to VT upon β-AR stimulation in *Pde4b*$^{-/-}$ mice. (**A**) Representative examples of simultaneous lead 1 ECG and intraventricular electrogram recordings obtained in WT and *Pde4b*$^{-/-}$ mice under Iso (0.2 mg/kg) after a burst of 30 stimuli at a cycle length (CL) of 55 ms. (**B** and **C**) Bar graphs showing the percentage of mice with arrhythmias induced (**B**) by burst pacing and (**C**) by 1 to 3 extrastimuli under baseline conditions and after intraperitoneal injections of Iso (0.02 mg/kg and 0.2 mg/kg). PES, paced extrasystole. *$P < 0.05$.

and contraction were enhanced in *Pde4b*$^{-/-}$ myocytes upon β-AR stimulation. This was accompanied by an accelerated relaxation and Ca^{2+} transient decay, although the latter did not quite reach statistical significance ($P = 0.059$ vs. WT). Accordingly, PLB phosphorylation and SR Ca^{2+} load tended to be increased during Iso stimulation in *Pde4b*$^{-/-}$ myocytes, but the differences with WT were not significant (Supplemental Figure 1). In addition, as shown in Supplemental Figure 2, PDE4B was anchored in macromolecular signaling complexes to $Ca_V1.2$ but not PLB or RyR2, and neither PLB phosphorylation at Ser-16 nor RyR2 phosphorylation at Ser-2808 were increased in *Pde4b*$^{-/-}$ hearts compared with that in WT hearts. Altogether, these results suggest that LTCCs constitute the primary target of PDE4B, although *Pde4b* ablation may not exclusively impact LTCC regulation. Interestingly, the absence of PDE4D also led to increased Ca^{2+} transients and contraction in mouse ventricular myocytes (Figure 7). Since, in these cells $I_{Ca,L}$ regulation was normal, the augmented ECC in *Pde4d*$^{-/-}$ myocytes could be related to PKA hyperphosphorylation of RyR2 during β-AR stimulation and increased open probability of the Ca^{2+} release channel (8, 29). However, increasing RyR activity alone may not be sufficient to explain an increase in Ca^{2+} transient amplitude (38), especially because such phenomenon can result ultimately in a decreased SR Ca^{2+} content (39, 40). PLB mediates part of the positive inotropic effect of β-AR stimulation by increasing SR Ca^{2+} load (41, 42). SR calcium content can by itself determine calcium transient amplitude independently from $I_{Ca,L}$ amplitude (38). A recent study indicates that PDE4D may also control PLB phosphorylation (30). Consistent with this idea, PLB phosphorylation was increased in *Pde4d*$^{-/-}$ myocytes under β-AR stimulation, and Iso more potently increased SR Ca^{2+} load in *Pde4d*$^{-/-}$ myocytes than in WT myocytes (Supplemental Figure 1). We propose that in *Pde4d*$^{-/-}$ myocytes both SR Ca^{2+} release and SR Ca^{2+} uptake are increased, leading to enhanced Ca^{2+} transients, while trigger activity remains unaltered. In this scheme, the unchanged decay kinetics of the Ca^{2+} transients in *Pde4d*$^{-/-}$ myocytes compared to those of WT myocytes under β-AR stimulation could be due to the balancing effect of increased diastolic Ca^{2+} leak and increased Ca^{2+} reuptake by the SR. Altogether, these results provide strong evidence that PDE4B and PDE4D isoforms differentially regulate cardiac ECC.

Alterations in Ca^{2+} handling are linked to cardiac arrhythmias (43). SCR events were increased in *Pde4d*$^{-/-}$ cells upon β-AR stimulation. These events were likely due to "leaky" hyperphosphorylated RyR2 channels that promote arrhythmias in mice invalidated for the *Pde4d* gene (29). Interestingly, inactivation of the *Pde4b* gene also favored SCR events in isolated cardiomyocytes upon β-AR stimulation, likely by a different mechanism. Therefore, PDE4B deficiency could lead to cardiac dysfunction and arrhythmias. This was further demonstrated in vivo using catheter-based ventricular stimulation that reliably induces ventricular arrhythmias (44). The susceptibility of WT and *Pde4b*$^{-/-}$ mice to the development VTs after paced extrasystoles or burst pacing was very low in baseline conditions. Interestingly, under β-AR stress, *Pde4b* inactivation significantly increased the incidence of arrhythmias induced by burst pacing but not by extrastimuli. In addition, no difference was detected between ECGs recorded from WT and *Pde4b*$^{-/-}$ mice. These results are consistent with triggered arrhythmias due to altered Ca^{2+} homeostasis rather than reentries or altered conduction. Arrhythmias triggered by burst pacing during β-AR stimulation could be due to early afterdepolarizations (EADs) or delayed afterdepolarizations (DADs) (43). Interestingly, increased β-AR stimulation also resulted in a larger shift of the activation curve of $I_{Ca,L}$ in *Pde4b*$^{-/-}$ myocytes. As a consequence, a larger window current would occur, promoting Ca^{2+} entry during the action

potential. Recovery from inactivation of $I_{Ca,L}$ within its window may provoke EADs during the action potential plateau (45–47). In addition, increased Ca^{2+} entry in cardiomyocytes could lead to Ca^{2+} overload and increase spontaneous SR Ca^{2+} release, thus promoting the occurrence of DADs. Future studies will be required to distinguish between these 2 possibilities.

In conclusion, our data identify PDE4B as an integral component of the LTCC complex and as the major PDE isoform regulating $I_{Ca,L}$ during β-AR stimulation. Consequently, PDE4B is crucial for the regulation of cardiac ECC and arrhythmogenesis. Interestingly, we recently reported that PDE4B expression and activity are decreased during cardiac hypertrophy (34). This could lead to increased phosphorylation of LTCC, as reported in failing human ventricular myocytes (48, 49), and therefore provide a mechanistic link to arrhythmias and sudden death in heart failure.

Methods

All experiments performed conformed to the European Community guiding principles in the care and use of animals (86/609/CEE), the local ethics committee (Comité Régional d'Ethique en matière d'Expérimentation Animale [CREEA] Ile-de-France Sud) guidelines, and the French decree no. 87–848. Approval for animal experiments according to this decree was obtained from the French Ministère de l'Agriculture, de la Pêche et de l'Alimentation (no. 92–283). Details concerning reagents, immunostaining, confocal imaging, electrophysiological experiments, ECG recording, intracardiac recording, and pacing can be found in the Supplemental Methods.

Preparation of mouse ventricular myocytes. Generation of *Pde4a*, *Pde4b*, and *Pde4d* homozygous null mice has been described previously (50). Ventricular myocytes were obtained from 5- to 6-month-old males with a mixed 129/Ola (25%) and C57BL/6 (75%) background. Animals were anesthetized by intraperitoneal injection of pentothal (150 mg/kg), and the heart was quickly removed and placed into a cold Ca^{2+}-free Tyrode's solution containing 113 mM NaCl, 4.7 mM KCl, 4 mM $MgSO_4$, 0.6 mM KH_2PO_4, 0.6 mM NaH_2PO_4, 10 mM BDM, 1.6 mM $NaHCO_3$, 10 mM HEPES, 30 mM Taurine, and 20 mM D-glucose, adjusted to pH 7.4. The ascending aorta was cannulated, and the heart was perfused with oxygenated Ca^{2+}-free Tyrode's solution at 37°C for 4 minutes using retrograde Langendorff perfusion. For enzymatic dissociation, the heart was perfused with Ca^{2+}-free Tyrode's solution containing Liberase TM Research Grade (Roche Diagnostics) for 10 minutes at 37°C. Then the heart was removed and placed into a dish containing Tyrode's solution supplemented with 0.2 mM $CaCl_2$ and 5 mg/ml BSA (Sigma-Aldrich). The ventricles were separated from the atria, cut into small pieces, and triturated with a pipette to disperse the myocytes. Ventricular myocytes were filtered on gauze and allowed to sediment by gravity for 10 minutes. The supernatant was removed, and cells were suspended in Tyrode's solution supplemented with 0.5 mM $CaCl_2$ and 5 mg/ml BSA. The procedure was repeated once, and cells were suspended in Tyrode's solution with 1 mM $CaCl_2$. Freshly isolated ventricular myocytes were plated in 35-mm culture dishes coated with laminin (10 μg/ml) and stored at room temperature until use. All experiments were performed at room temperature within 6 hours after cell isolation.

Preparation of protein extracts. Frozen adult mouse hearts or isolated AMVMs were homogenized in ice-cold buffer containing 150 mM NaCl, 20 mM HEPES (pH 7.4), 2 mM EDTA, and 0.2 mM EGTA and supplemented with 10% glycerol, 1% Triton X-100, 1 μM microcystin-LR, and Complete Protease Inhibitor Tablets (Roche Diagnostics). Tissue lysates were centrifuged at 20,000 *g* and 4°C for 20 minutes, and supernatants were either used directly for PDE activity assays or Western blotting or were first subjected to IPs as described below.

IP. IP of PDE4 subtypes was performed as described previously (24). In brief, cell and tissue extracts, prepared as described in "Preparation of protein extracts," were precleared for 1 hour using 50 μl protein G-Sepharose, followed by a second centrifugation at 20,000 *g* and 4°C for 10 minutes. Precleared detergent extracts were then immunoprecipitated using 10 μg of the respective anti-PDE4 antibody or 10 μg of control IgG for 2 hours at 4°C. IP of $Ca_V1.2$, RyR2, and PLB was performed under similar conditions as described in more detail previously (7, 24, 29).

PDE assay. Cyclic AMP-PDE activity was measured according to the method of Thompson and Appleman as described previously (51). In brief, samples were assayed in a 200-μl reaction mixture containing 40 mM Tris-HCl (pH 8.0), 1 mM $MgCl_2$, 1.4 mM β-mercaptoethanol, 1 μM cAMP, 0.75 mg/ml bovine serum albumin, and 0.1 μCi of [^{3}H]cAMP for 30 minutes at 33°C. The reaction was terminated by heat inactivation in a boiling water bath for 1 minute. The PDE reaction product 5′-AMP was then hydrolyzed by incubation of the assay mixture with 50 μg *Crotalus atrox* snake venom for 20 minutes at 33°C, and the resulting adenosine was separated by anion exchange chromatography using 1 ml AG1-X8 resin (Bio-Rad) and quantified by scintillation counting. PDE4 activity was defined as the fraction of cAMP-PDE activity inhibited by 10 μM rolipram.

Electrophysiological experiments. The whole-cell configuration of the patch-clamp technique was used to record $I_{Ca,L}$. Patch electrodes with 1–2 MΩ resistance when filled with internal solution contained 118 mM CsCl, 5 mM EGTA, 4 mM $MgCl_2$, 5 mM sodium phosphocreatine, 3.1 mM Na_2ATP, 0.42 mM Na_2GTP, 0.062 mM $CaCl_2$ (pCa 8.5), and 10 mM HEPES, adjusted to pH 7.3. External Cs^+-Ringer solution contained 107.1 mM NaCl, 20 mM CsCl, 4 mM $NaHCO_3$, 0.8 mM NaH_2PO_4, 5 mM D-glucose, 5 mM sodium pyruvate, 10 mM HEPES, 1.8 mM $MgCl_2$, and 1.8 mM $CaCl_2$, adjusted to pH 7.4. The cells were depolarized every 8 seconds from –50 mV to 0 mV for 400 ms. The use of –50 mV as holding potential allowed the inactivation of voltage-dependent sodium currents. Potassium currents were blocked by replacing all K^+ ions with external and internal Cs^+. The current-voltage relationship and steady-state inactivation properties were measured by applying a 200-ms pulse from –60 to +60 mV, followed by a 3-ms repolarization to –50 mV, before the 200-ms test pulse to 0 mV.

Measurements of Ca^{2+} transients and cell shortening. Isolated cardiomyocytes were loaded with 5 μM Fura-2 AM (Invitrogen) at room temperature for 15 minutes and then washed with external Ringer solution containing 121.6 mM NaCl, 5.4 mM KCl, 4.013 mM $NaHCO_3$, 0.8 mM NaH_2PO_4, 10 mM HEPES, 5 mM glucose, 5 mM Na pyruvate, 1.8 mM $MgCl_2$, and 1 mM $CaCl_2$, pH 7.4. The loaded cells were field stimulated (5 V, 4 ms) at a frequency of 0.5 Hz. SL and Fura-2 ratio (measured at 512 nm upon excitation at 340 nm and 380 nm) were simultaneously recorded using an IonOptix System (IonOptix). Cell contractility was assessed by the percentage of sarcomere shortening, which is the ratio of twitch amplitude (difference of end-diastolic and peak systolic SL) to end-diastolic SL. Ca^{2+} transients were assessed by the percentage of variation of the Fura-2 ratio by dividing the twitch amplitude (difference of end-diastolic and peak systolic ratios) to end-diastolic ratio. The $t_{1/2off}$ was used as an index of relaxation and Ca^{2+} transient decay kinetics. All parameters were calculated offline using a dedicated software (IonWizard 6x).

Immunocytochemistry. Cardiomyocytes were permeabilized after fixation with 0.25% Triton X-100 and probed with rabbit polyclonal anti-$Ca_V1.2$ antibody (CNC1, ref. 52) and mouse monoclonal anti–α-actinin or rabbit antibody 113-4 raised against the C terminus of PDE4B and mouse monoclonal anti–α-actinin.

ECG recording and intracardiac recording and pacing. ECG recording was performed as previously described on mice anesthetized by intraperitoneal injection of etomidate (32 mg/kg; Janssen-Cilag) (53). After ECG recording, the extremity of a 2F octapolar catheter (Biosense Webster) was placed

in the right ventricle through the right internal jugular vein. Standard pacing protocols were used to determine the VERPs and to induce ventricular arrhythmias. The inducibility of ventricular arrhythmias was assessed in baseline condition and after intraperitoneal infusions of Iso (0.02 mg/kg and 0.2 mg/kg) by using the programmed electrical stimulation method with 1 to 3 extrastimuli (performed twice) and burst pacing. VT was defined as the occurrence after the last paced beat of at least 4 consecutive QRS complexes with a different morphology from that seen in normal sinus rhythm. VT of more than 10 cycles was defined as sustained VT.

Statistics. Data are represented as mean ± SEM. Statistics were performed using Excel and the StatXact 8 softwares. Statistical significance was evaluated using Student's 2-tailed unpaired *t* test and Barnard's exact test. A difference was considered statistically significant when P was < 0.05.

Acknowledgments

The authors wish to thank Agnès Hivonnait (INSERM UMR915, Cardiex facility, Nantes) for technical assistance in ECG and intracardiac recording and pacing, Patrick Lechêne (INSERM U769) for help with data analysis, Pauline Robert and Valérie Domergue-Dupont (animal core facility, University Paris-Sud, IFR141) for handling and genotyping of mice, and Valérie Nicolas (imaging core facility, University Paris-Sud, IFR141) for technical assistance with confocal microscopy. Cardiex facility is supported by the GIS-IBiSA program. This work was supported by Leducq cycAMP grant 06CVD02 (to R. Fischmeister and M. Conti), European Union contract LSHM-CT-2005-018833/EUGeneHeart (to R. Fischmeister), NIH grant HL092788 (to M. Conti), NIH grant R01 HL085372 (to W.A. Catterall), the Fondation Lefoulon-Delalande (to J. Leroy), the Fondation de France (to G. Vandecasteele), and Agence Nationale de la Recherche grant 2010 BLAN 1139 01 (to G. Vandecasteele).

Received for publication August 13, 2010, and accepted in revised form April 20, 2011.

Address correspondence to: Rodolphe Fischmeister or Grégoire Vandecasteele, INSERM UMR-S 769, Université Paris-Sud, Faculté de Pharmacie, 5, Rue J.-B. Clément, F-92296 Châtenay-Malabry Cedex, France. Phone: 33.1.46.83.57.57; Fax 33.1.46.83.54.75; E-mail: rodolphe.fischmeister@inserm.fr (R. Fischmeister), gregoire.vandecasteele@u-psud.fr (G. Vandecasteele).

1. Bers DM. Cardiac excitation-contraction coupling. *Nature*. 2002;415(6868):198–205.
2. Catterall WA. Structure and regulation of voltage–gated Ca^{2+} channels. *Annu Rev Cell Dev Biol*. 2000;16:521–555.
3. Fuller MD, Emrick MA, Sadilek M, Scheuer T, Catterall WA. Molecular mechanism of calcium channel regulation in the fight-or-flight response. *Sci Signal*. 2010;3(141):ra70.
4. Haase H, et al. Ahnak is critical for cardiac Ca(V)1.2 calcium channel function and its beta-adrenergic regulation. *FASEB J*. 2005;19(14):1969–1977.
5. Bunemann M, Gerhardstein BL, Gao TY, Hosey MM. Functional regulation of L-type calcium channels via protein kinase A-mediated phosphorylation of the β_2 subunit. *J Biol Chem*. 1999;274(48):33851–33854.
6. Fraser IDC, et al. A novel lipid-anchored A-kinase anchoring protein facilitates cAMP-responsive membrane events. *EMBO J*. 1998;17(8):2261–2272.
7. Hulme JT, Lin TW, Westenbroek RE, Scheuer T, Catterall WA. β-Adrenergic regulation requires direct anchoring of PKA to cardiac $Ca_v1.2$ channels via a leucine zipper interaction with A kinase-anchoring protein 15. *Proc Natl Acad Sci U S A*. 2003;100(22):13093–13098.
8. Marx SO, et al. PKA phosphorylation dissociates FKBP12.6 from the calcium release channel (Ryanodine receptor): Defective regulation in failing hearts. *Cell*. 2000;101(4):365–376.
9. Kapiloff MS, Jackson N, Airhart N. mAKAP and the ryanodine receptor are part of a multi-component signaling complex on the cardiomyocyte nuclear envelope. *J Cell Sci*. 2001;114(pt 17):3167–3176.
10. Lygren B, et al. AKAP complex regulates Ca^{2+} reuptake into heart sarcoplasmic reticulum. *EMBO Rep*. 2007;8(11):1061–1067.
11. Steinberg SF, Brunton LL. Compartmentation of G protein–coupled signaling pathways in cardiac myocytes. *Annu Rev Pharmacol Toxicol*. 2001;41:751–773.
12. Fischmeister R, et al. Compartmentation of cyclic nucleotide signaling in the heart: The role of cyclic nucleotide phosphodiesterases. *Circ Res*. 2006; 99(8):816–828.
13. Patrucco E, Albergine MS, Santana LF, Beavo JA. Phosphodiesterase 8A (PDE8A) regulates excitation-contraction coupling in ventricular myocytes. *J Mol Cell Cardiol*. 2010;49(2):330–333.
14. Rochais F, et al. A specific pattern of phosphodiesterases controls the cAMP signals generated by different G_s-coupled receptors in adult rat ventricular myocytes. *Circ Res*. 2006;98(8):1081–1088.
15. Rochais F, et al. Negative feedback exerted by PKA and cAMP phosphodiesterase on subsarcolemmal cAMP signals in intact cardiac myocytes. An *in vivo* study using adenovirus-mediated expression of CNG channels. *J Biol Chem*. 2004;279(50):52095–52105.
16. Mongillo M, et al. Fluorescence resonance energy transfer-based analysis of cAMP dynamics in live neonatal rat cardiac myocytes reveals distinct functions of compartmentalized phosphodiesterases. *Circ Res*. 2004;95(1):67–75.
17. Xiang Y, Naro F, Zoudilova M, Jin SL, Conti M, Kobilka B. Phosphodiesterase 4D is required for β_2 adrenoceptor subtype-specific signaling in cardiac myocytes. *Proc Natl Acad Sci U S A*. 2005;102(3):909–914.
18. Leroy J, et al. Spatiotemporal dynamics of β-adrenergic cAMP signals and L-type Ca^{2+} channel regulation in adult rat ventricular myocytes: Role of phosphodiesterases. *Circ Res*. 2008;102(9):1091–1100.
19. Nikolaev VO, Bunemann M, Schmitteckert E, Lohse MJ, Engelhardt S. Cyclic AMP imaging in adult cardiac myocytes reveals far-reaching β_1-adrenergic but locally confined β_2-adrenergic receptor-mediated signaling. *Circ Res*. 2006;99(10):1084–1091.
20. Verde I, Vandecasteele G, Lezoualc'h F, Fischmeister R. Characterization of the cyclic nucleotide phosphodiesterase subtypes involved in the regulation of the L-type Ca^{2+} current in rat ventricular myocytes. *Br J Pharmacol*. 1999;127(1):65–74.
21. Kostic MM, et al. Altered expression of PDE1 and PDE4 cyclic nucleotide phosphodiesterase isoforms in 7-oxo-prostacyclin-preconditioned rat heart. *J Mol Cell Cardiol*. 1997;29(11):3135–3146.
22. Bolger GB, Conti M, Houslay MD. Cellular functions of PDE4 enzymes. In: Francis S, Beavo JA, Houslay MD, eds. *Cyclic Nucleotide Phosphodiesterases in Health and Disease*. Florence, Kentucky, USA: CRC Press, Taylor and Francis Group; 2007:99–130.
23. Richter W, Jin SL, Conti M. Splice variants of the cyclic nucleotide phosphodiesterase PDE4D are differentially expressed and regulated in rat tissue. *Biochem J*. 2005;388(pt 3):803–811.
24. Richter W, Xie M, Scheitrum C, Krall J, Movsesian MA, Conti M. Conserved expression and functions of PDE4 in rodent and human heart. *Basic Res Cardiol*. 2011;106(2):249–62.
25. Baillie GS, et al. β-Arrestin-mediated PDE4 cAMP phosphodiesterase recruitment regulates β-adrenoceptor switching from G_s to G_i. *Proc Natl Acad Sci U S A*. 2003;100(3):940–945.
26. Richter W, et al. Signaling from β_1- and β_2-adrenergic receptors is defined by differential interactions with PDE4. *EMBO J*. 2008;27(2):384–393.
27. De Arcangelis V, Liu R, Soto D, Xiang Y. Differential association of phosphodiesterase 4D isoforms with β_2-adrenoceptor in cardiac myocytes. *J Biol Chem*. 2009;284(49):33824–33832.
28. Terrenoire C, Houslay MD, Baillie GS, Kass RS. The cardiac I_{Ks} potassium channel macromolecular complex includes the phosphodiesterase PDE4D3. *J Biol Chem*. 2009;284(14):9140–9146.
29. Lehnart SE, et al. Phosphodiesterase 4D deficiency in the ryanodine receptor complex promotes heart failure and arrhythmias. *Cell*. 2005;123(1):25–35.
30. Kerfant BG, et al. PI3KY is required for PDE4, not PDE3, activity in subcellular microdomains containing the sarcoplasmic reticular calcium ATPase in cardiomyocytes. *Circ Res*. 2007;101(4):400–408.
31. De Jongh KS, Murphy BJ, Colvin AA, Hell JW, Takahashi M, Catterall WA. Specific phosphorylation of a site in the full-length form of the α1 subunit of the cardiac L-type calcium channel by adenosine 3′,5′-cyclic monophosphate-dependent protein kinase. *Biochemistry*. 1996;35(32):10392–10402.
32. Gao T, Puri TS, Gerhardstein BL, Chien AJ, Green RD, Hosey MM. Identification and subcellular localization of the subunits of L-type calcium channels and adenylyl cyclase in cardiac myocytes. *J Biol Chem*. 1997;272(31):19401–19407.
33. Kajimoto K, Hagiwara N, Kasanuki H, Hosoda S. Contribution of phosphodiesterase isozymes to the regulation of the L-type calcium current in human cardiac myocytes. *Br J Pharmacol*. 1997; 121(8):1549–1556.
34. Abi-Gerges A, et al. Decreased expression and activity of cAMP phosphodiesterases in cardiac hypertrophy and its impact on β-adrenergic cAMP signals. *Circ Res*. 2009;105(8):784–792.
35. Balijepalli RC, Foell JD, Hall DD, Hell JW, Kamp TJ. Localization of cardiac L-type Ca^{2+} channels to a caveolar macromolecular signaling complex is required for β_2-adrenergic regulation. *Proc Natl Acad Sci U S A*. 2006;103(19):7500–7505.
36. Nichols CB, et al. Sympathetic stimulation of adult cardiomyocytes requires association of AKAP5 with a subpopulation of L-type calcium channels. *Circ Res*. 2010;107(6):747–756.
37. Callewaert G, Cleemann L, Morad M. Epinephrine enhances Ca^{2+} current-regulated Ca^{2+} release and Ca^{2+} reuptake in rat ventricular myocytes. *Proc Natl Acad Sci U S A*. 1988;85(6):2009–2013.
38. Ginsburg KS, Bers DM. Modulation of excitation-contraction coupling by isoproterenol in cardio-

myocytes with controlled SR Ca^{2+} load and Ca^{2+} current trigger. *J Physiol*. 2004;556(pt 2):463–480.
39. Trafford AW, Diaz ME, Sibbring GC, Eisner DA. Modulation of CICR has no maintained effect on systolic Ca^{2+}: simultaneous measurements of sarcoplasmic reticulum and sarcolemmal Ca^{2+} fluxes in rat ventricular myocytes. *J Physiol*. 2000;522(pt 2):259–270.
40. Eisner DA, Kashimura T, O'Neill SC, Venetucci LA, Trafford AW. What role does modulation of the ryanodine receptor play in cardiac inotropy and arrhythmogenesis? *J Mol Cell Cardiol*. 2009; 46(4):474–481.
41. Wolska BM, Stojanovic MO, Luo W, Kranias EG, Solaro RJ. Effect of ablation of phospholamban on dynamics of cardiac myocyte contraction and intracellular Ca2+. *Am J Physiol*. 1996; 271(1 pt 1):C391–C397.
42. Santana LF, Kranias EG, Lederer WJ. Calcium sparks and excitation-contraction coupling in phospholamban-deficient mouse ventricular myocytes. *J Physiol*. 1997;503(pt 1):21–29.
43. Pogwizd SM, Bers DM. Cellular basis of triggered arrhythmias in heart failure. *Trends Cardiovasc Med*. 2004;14(2):61–66.
44. Gellen B, et al. Conditional FKBP12.6 overexpression in mouse cardiac myocytes prevents triggered ventricular tachycardia through specific alterations in EC coupling. *Circulation*. 2008;117(14):1778–1786.
45. January CT, Riddle JM. Early after depolarizations — Mechanism of induction and block — A role for L-type Ca^{2+} current. *Circ Res*. 1989;64(5):977–990.
46. Wu Y, et al. Calmodulin kinase II and arrhythmias in a mouse model of cardiac hypertrophy. *Circulation*. 2002;106(10):1288–1293.
47. Koval OM, et al. CaV1.2 beta-subunit coordinates CaMKII-triggered cardiomyocyte death and afterdepolarizations. *Proc Natl Acad Sci U S A*. 2010; 107(11):4996–5000.
48. Schroder F, et al. Increased availability and open probability of single L-type calcium channels from failing compared with nonfailing human ventricle. *Circulation*. 1998;98(10):969–976.
49. Chen X, Piacentino V 3rd, Furukawa S, Goldman B, Margulies KB, Houser SR. L-type Ca^{2+} channel density and regulation are altered in failing human ventricular myocytes and recover after support with mechanical assist devices. *Circ Res*. 2002;91(6):517–524.
50. Jin SL, Latour AM, Conti M. Generation of PDE4 knockout mice by gene targeting. *Methods Mol Biol*. 2005;307:191–210.
51. Richter W, Conti M. Dimerization of the type 4 cAMP-specific phosphodiesterases is mediated by the upstream conserved regions (UCRs). *J Biol Chem*. 2002;277(43):40212–40221.
52. Hulme JT, Westenbroek RE, Scheuer T, Catterall WA. Phosphorylation of serine 1928 in the distal C-terminal domain of cardiac $Ca_v1.2$ channels during β1-adrenergic regulation. *Proc Natl Acad Sci U S A*. 2006;103(44):16574–16579.
53. Royer A, et al. Mouse model of SCN5A-linked hereditary Lenegre's disease: age-related conduction slowing and myocardial fibrosis. *Circulation*. 2005; 111(14):1738–1746.